The Lowest Photoexcited Triplet State of Subphthalocyanine in Solid and Fluid Environments. Time-Resolved Electron Paramagnetic Resonance Studies

Seigo Yamauchi,*,† Akihiro Takahashi,† Yohei Iwasaki,† Masashi Unno,† Yasunori Ohba,† Jiro Higuchi,‡ Aharon Blank,§ and Haim Levanon*,§

Institute of Multidisciplinary Research for Advanced Materials, Tohoku University, Sendai 980-8577, Japan, Department of Applied Chemistry, Graduate School of Engineering, Yokohama National University, Yokohama 790-9826, Japan, and Department of Physical Chemistry and the Farkas Center for Light-Induced Processes, The Hebrew University, Jerusalem 91904, Israel

Received: March 24, 2002; In Final Form: October 2, 2002

Time-resolved EPR spectra of the lowest excited triplet state of boron subphthalocyanine chloride have been measured in toluene at various temperatures (5−360 K). On the basis of the observed and simulated spectra, electronic structure and molecular motion of the triplet state (^{1}T) were analyzed, both in solid and fluid solution. The simulations were carried out using a model, which considers a temperature-dependent exchange between sites having different zero-field splitting (ZFS) parameters and molecular orientations. The ZFS parameter, *D*, was nearly the same at all temperatures examined. At very low temperatures, below 20 K, the spectrum was analyzed by a static model. At 40−120 K, two conformers with different ZFS parameter, *E*, have been found. The population ratio between the two conformers showed strong temperature dependence. These conformers were attributed to Jahn−Teller states and were identified by their different ZFS parameters. The exchange rate and activation energy of the conformers were compared with similar experiments performed in solid solution. Further increase in temperature (130−160 K) resulted in noticeable change in the spectra. However, at this temperature range the spectra could not be analyzed quantitatively because of the unstable crystal structure of toluene (soft glass). Above 163 K, the solvent turns slowly into fluid and the spectra were strongly dependent upon temperature. In this range of temperatures, molecular rotations occur, initially around the out-of-plane *z*-axis, and, as temperature rises, also around the in-plane *x*- and *y*-axes. Anisotropic exchange rates were obtained from the spectral simulation and were analyzed by a population exchange between the Jahn−Teller states combined with anisotropic rotations. Anisotropic spin−lattice (T_1) and spin−spin (T_2) relaxation times were also obtained and discussed. The rotations become isotropic above 263 K, where the spectrum exhibits a single sharp Lorentzian line and is analyzed in terms of the dipolar spin interaction.

1. Introduction

The lowest excited triplet (^{1}T) state was studied and analyzed extensively at low temperatures in rigid environments by means of time-resolved EPR (TREPR) technique.[1] These measurements utilized the strong electron spin polarization of the ^{1}T state to obtain the EPR signal. Until recent years, the EPR spectra of the ^{1}T state (as opposed to stable biradicals[2]) in fluid solution had not been observed. Nevertheless, there were several examinations of the behavior of ^{1}T for molecules at high temperatures in materials such as plastics,[3] single[4] and liquid[5] crystals, polymers,[6] biological in vivo systems,[7] and even glasses.[8,9] In these studies, the authors analyzed the temperature dependence of the signal decay, ZFS parameters, and the exchange rates between sites. The results were interpreted in terms of the mobility of the environments, involvement of higher excited triplet states and different conformers, and changes in the electronic structures.

In 1992, the first observation of the ^{1}T signal was reported for fullerene ($^3C_{60}$*)[1] in fluid solution (toluene),[1,5,10] measured by TREPR, where the slow triplet spin relaxation rate in fluid allowed to obtain the EPR spectra. In 1994, McLauchlan et al. reported the TREPR spectra of "trapped triplet anthracene" in fluid solution.[11] Although the species involved were not completely assigned, the analysis of the spectra, which exhibits asymmetry and the temperature-dependent line width in solution, is of interest to our work. In parallel to these pioneering experiments, attempts to observe ^{1}T spectra with complex line shape were performed. Recently, we have succeeded in observing the ^{1}T spectra of metalloporphyrins (MPors)[12] and metallophthalocyanines (MPcs).[13] These molecules are characterized by broad spectra (>7 mT), as compared to fullerene (∼0.05 mT at room temperature). In fullerene, spin relaxation of the ^{1}T state was analyzed by employing pulsed EPR, and the electronic structure and molecular dynamics were deduced from the relaxation rates.[14] However, as will be shown here, these static and dynamic parameters can be extracted directly from the spectral simulation.

Up-to-date, two major models have been reported and tested for the simulation of the ^{1}T spectrum in soft media. The first is the discrete jump model[15] and the second is the rotational

* To whom correspondence should be addressed. Fax: 81-22-217-5616; tel: 81-22-217-5617; e-mail: yamauchi@tagen.tohoku.ac.jp.
† Tohoku University.
‡ Yokohama National University.
§ The Hebrew University.

10.1021/jp0258210 CCC: $25.00
Published on Web 02/15/2003

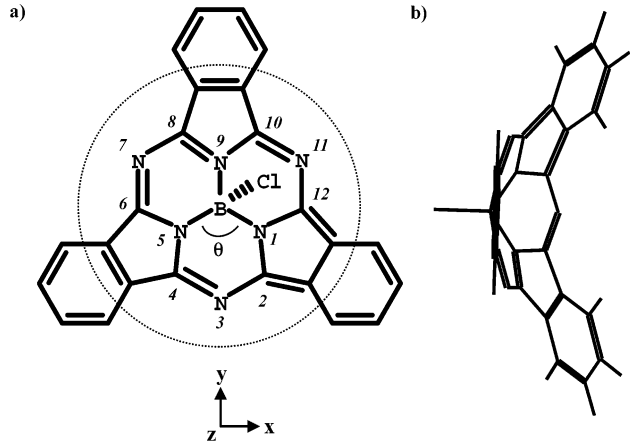

Figure 1. (a) Molecular structure and (b) calculated optimum geometry of boron subpthalocyanine chloride. Refer to the text for a dotted circle and numbering of the atoms.

diffusion model.[16] The former usually provides better fit of the observed line shape at low temperatures, while the latter usually provides better fit at high temperatures in liquid environments.[17]

In this study, boron (III) subphthalocyanine chloride (SubPc; Figure 1) was chosen, since this molecule is smaller than the porphyrins and phthalocyanines studied previously and also since it has a unique structure of C_{3v} symmetry. In addition, SubPc derivatives have been utilized as intermediates in synthesizing unique phthalocyanines,[18,19] materials of nonlinear (second and third harmonics) optical properties,[20] and optical recording media.[21]

TREPR spectra of the ^{1}T state of SubPc were observed in toluene at various temperatures (5−360 K) and simulated in terms of the excited states dynamics and molecular motions both in solid and fluid solution. The spectral simulation was carried out with a model that considers two sites or more, having different magnetic parameters and intersystem crossing rates. These sites are exchangeable and can rotate with temperature-dependent rates. Such a behavior is typically realized in the molecules having high symmetry, for example, SubPc and metalloporphyrins.

2. Experimental Section

SubPc was purchased from Aldrich Co. and purified by column chromatography. The purity of the sample was checked by UV/vis absorption (Shimadzu UV-240 spectrometer), elementary analysis, and ^{1}H NMR (Bruker MSL300). Spectral-grade toluene was purchased from Nakarai Tasque Co. and was used as solvent without further purification. The concentration of the sample was 0.3 mM. In the EPR experiment, the sample was deaerated by Ar gas bubbling and flowed through a microwave cavity.

EPR signals were recorded using a modified X-band JEOL JES-FE2XG spectrometer, where the bandwidth of the amplifier is ca. 20 MHz. Decay curves of transient EPR signals were accumulated at every magnetic field on an Iwatsu DM-7200 digital memory using a sample rate of 10 ns and stored in the computer. The analysis resulted in two-dimensional EPR spectra with respect to the magnetic field and time after the laser pulse. A boxcar integrator (NF-BX-531) was also utilized in the observations of time-resolved EPR spectra with an appropriate time gate width (100−200 ns). The time resolution of our EPR system is ca. 80 ns.

Temperature was controlled using a JEOL ES-DVT3 nitrogen gas flow system or an Oxford ESR 900 helium gas flow system. The molecule was excited at 550 nm with a Spectra Physics GCR −170 OPO laser, pumped by a GCR-170 Nd:YAG laser. The output power and the repetition rate of the laser were 10 mJ/pulse and 10 Hz, respectively.

MO calculations were made using the semiempirical AM-1 and ab initio methods in the Gaussian 98 program with the B3LYP functional using 3-21G and 6-31G* basis sets.[22] The geometry of the X-ray structural analysis[23] was used as starting geometry and was further optimized by the calculation.

3. Simulation of Triplet EPR Spectra

To model accurately the EPR line shape of the triplet over a wide temperature range, we employed an advanced line shape simulation, which is an improvement of our previous approach.[15] The new simulation can treat the case of N different molecular conformers, which can exchange energy between them. Thus, for example, for $N = 4$, the calculation time of the spectra is ∼ 30 min (for Pentium III computer). Larger N values would require longer calculation times or better computer resources. Each species may have its own ZFS parameters (D and E), anisotropic spin relaxation times (T_{1x}, T_{1y}, T_{1z}, T_{2x}, T_{2y}, T_{2z}), and anisotropic selective levels population (A_x, A_y, A_z). In addition, each species may have its own orientation in the magnetic field relative to a specified orientation of the first treated species, which enables the consideration of "discrete jumps" between different possible orientations.[15] A general matrix, which describes the coupling between the various species, can also be accounted for. The simulation is performed numerically with a Matlab routine, which provides convenient graphical interface and also enables efficient multiparameter optimization to provide the set of parameters, which best describes the experimental spectra.

The algorithm uses the early basic ideas for the exchange mechanism between the species.[24] In addition, it employs the general form of the discrete jumps model[14] and the selective triplet levels population.[25]

The relevant triplet spin Hamiltonian is given by

$$\mathscr{H} = g\beta S\cdot B_0 + S\cdot\mathbf{D}\cdot S \tag{1}$$

which can be written also as

$$\mathscr{H} = g\beta S\cdot B_0 + \mathbf{D}\left\{S^2_z - \frac{1}{3}S(S+1)\right\} + E(S^2_x - S^2_y) \tag{2}$$

where

$$\mathbf{D} = \mathbf{D}_{zz} - \frac{1}{2}(\mathbf{D}_{xx} + \mathbf{D}_{yy}) \tag{3}$$

$$E = \frac{1}{2}(\mathbf{D}_{xx} - \mathbf{D}_{yy}) \tag{4}$$

and $\mathbf{D}_{ii}$ are the components of the **D** tensor as presented in eq 1, and the hyperfine term is neglected.

The high-field wave functions $|+1>$, $|0>$, $|-1>$ diagonalize the Zeeman part of the Hamiltonian. To diagonalize the full Hamiltonian, we use a standard procedure in which we first neglect D and E (which are ∼10 times smaller than the Zeeman interaction) to obtain the eigenvectors:[26]

$$\begin{pmatrix}\Sigma_1\\ \Sigma_2\\ \Sigma_3\end{pmatrix} =$$

$$\begin{pmatrix} \frac{1}{2}(l-im)\left[\frac{1+n}{1-n}\right]^{1/2} & \sqrt{2}(1-n^2)^{1/2} & \frac{1}{2}(l+im)\left[\frac{1-n}{1+n}\right]^{1/2} \\ -\sqrt{2}(l-im) & n & \sqrt{2}(l+im) \\ \frac{1}{2}(l-im)\left[\frac{1-n}{1+n}\right]^{1/2} & -\sqrt{2}(1-n^2)^{1/2} & \frac{1}{2}(l+im)\left[\frac{1+n}{1-n}\right]^{1/2} \end{pmatrix} \begin{pmatrix}|1\rangle\\ |0\rangle\\ |-1\rangle\end{pmatrix} \quad (5)$$

After that we insert D and E as a first-order perturbation to obtain the diagonal Hamiltonian matrix:[26]

$$H = \begin{bmatrix} -\frac{D}{6}(1-3n^2) + \frac{E}{2}(l^2-m^2) + \omega_0 & 0 & 0 \\ 0 & \frac{D}{3}(1-3n^2) - E(l^2-m^2) & 0 \\ 0 & 0 & -\frac{D}{6}(1-3n^2) + \frac{E}{2}(l^2-m^2) - \omega_0 \end{bmatrix} \quad (6)$$

where $l = \sin\theta\cos\phi$; $m = \sin\theta\sin\phi$; $n = \cos\theta$, for the spatial angle, θ, ϕ, which describe the direction of B_0 with respect to the molecular z-axis. Thus, the energy levels depend on the molecular orientation in the external magnetic field, resulting in a broad inhomogeneous spectrum for isotropically distributed molecular orientations.

Let us consider the case of N different triplet species (with different Hamiltonian) in the same solution, which interact with each other. Different Hamiltonians imply that each species may be in a different orientation (similar to the regular discrete jump model)[27] but also may have different ZFS parameters D, E. The spin distribution of each species is described by the density matrix ρ_A, ρ_B, and so forth. For each species, we may write the following Liouville equation:

$$\frac{d\rho_A}{dt} = i[\rho_A,\mathscr{H}_A] + \sum_B (P_{BA}\rho_B - P_{AB}\rho_A) - \hat{\mathbf{R}}_\mathbf{A}(\boldsymbol{\rho}_\mathbf{A} - \boldsymbol{\rho}_{\mathbf{A}_0}) \quad (7)$$

where $\mathscr{H}_A$ is the Hamiltonian of species A, P_{AB} is the exchange rate of from A to B, $\hat{R}_A$ is a generalized Redfield relaxation matrix, and ρ_{A_0} is the "steady-sate" density matrix. Following Hudson and McLachlan's approach,[24] which relies on the extensive treatment of Kubo and Tomita,[28] we can write the solution of eq 7 for the line shape intensity I versus ω for a given DC field as

$$I(\omega) = 2\,Im\,Tr\left\{\rho_0 S_x\left[\frac{1}{(\hat{\Omega} - \omega - i(\hat{\Pi} + \hat{\mathbf{R}})}\right]S_x\right\} \quad (8)$$

where ρ_0 is the steady-state density matrix for all the species. Unlike the original treatment,[24] where ρ_0 describes the thermal triplet population, in the present case it describes a spin polarized triplet and includes also the effect of thermal relaxation (T_1).[29,30]

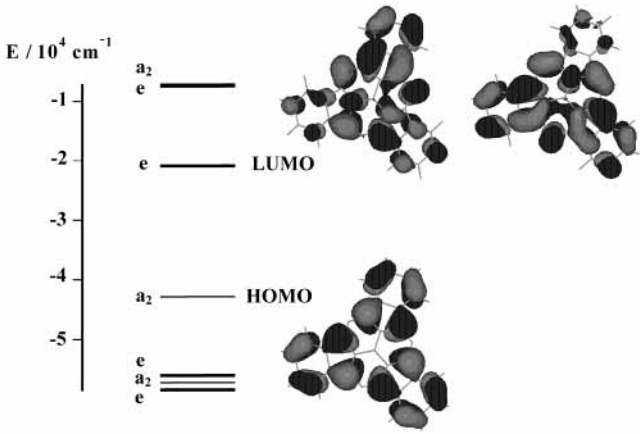

Figure 2. Calculated energy levels near HOMO and electron distribution of LUMO and HOMO by use of ab initio calculation with B3LPY/6-31G*.

The term S_x is the matrix presentation for the Heisenberg spin operator of the triplet, $\hat{\Omega}$ is a 9N ⊗ 9N supermatrix representing the commutator operator in eq 7, for the Hamiltonian of different sites, and the supermatrixes $\hat{\Pi}$ and $\hat{\mathbf{R}}$ are related to the exchange and the relaxation processes, respectively.

Equation 8 is solved numerically for each ω and molecular orientation (l, m, n). At this point one can also insert a distribution function, which determines the distribution of orientations for the triplet molecule. For example, one may use isotropic distribution for isotropic solvents or other types of distributions for anisotropic environments, such as liquid crystals.

4. Results

a. Electronic Structure of the Excited State. Energy levels and wave functions of the MOs were calculated by the two methods mentioned in section 2. Typical results of the B3LPY/6-31G* calculation are shown in Figure 2, giving a nonplanar ammonia-type structure, as shown in Figure 1b. The ordering of the MOs near the HOMO (110) and the LUMO (111 and 112) does not depend on the calculation method, while the energy difference between the HOMO and the LUMO depends remarkably on the method and the basis set. When the 6-31G* basis set and B3LPY hybrid functional are used, the energy difference between HOMO and LUMO is 2.8 eV (439 nm), which corresponds to the energy of the lowest excited singlet (^{1}S) state (565 nm) obtained from the UV/vis absorption spectrum.[18,19] It was found from Figure 2 that HOMO belongs to a_2 symmetry and LUMO to e, in the C_{3v} point group. As these two MOs are located apart from the other MOs in all calculations examined, the ^{1}S and ^{1}T states must be composed mostly of single E (a_2−e) configuration and might suffer from a Jahn−Teller distortion. The electronic structures of the two LUMOs result in molecular shapes of isosceles triangles with short (S) and long (L) bases, which are just those expected from the Jahn−Teller distortion in the ^{1}S and ^{1}T states.

b. Calculation of the Zero-Field Splitting Parameters. The ZFS parameters D and E were calculated for the excited triplet states of SubPc by two methods, using eqs 9 and 10.

$$D = (-3/4)(\mu_0/4\pi)(g\beta)^2 \int \psi_{1T}[(3z^2 - R^2)/R^5]\,\psi_{1T}\,dv_1 dv_2 \quad (9)$$

$$E = (-3/4)(\mu_0/4\pi)(g\beta)^2 \int \psi_{1T}[(x^2 - y^2)/R^5]\,\psi_{1T}\,dv_1 dv_2 \quad (10)$$

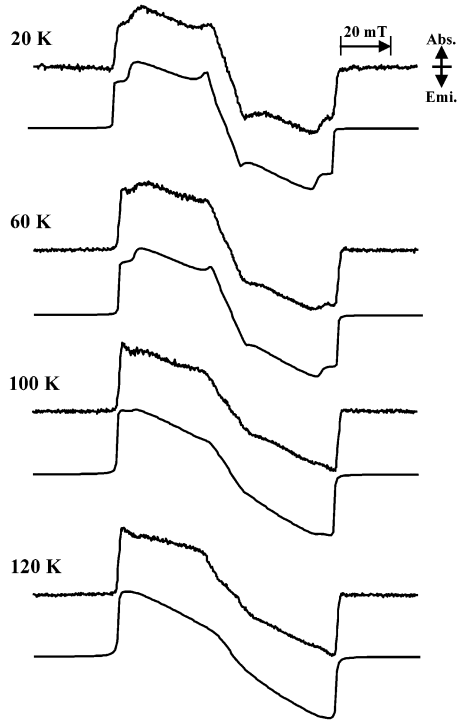

Figure 3. Experimentally obtained and simulated time-resolved EPR spectra of boronsubpthalocyanine chloride in the excited triplet state at 20−120 K in toluene.

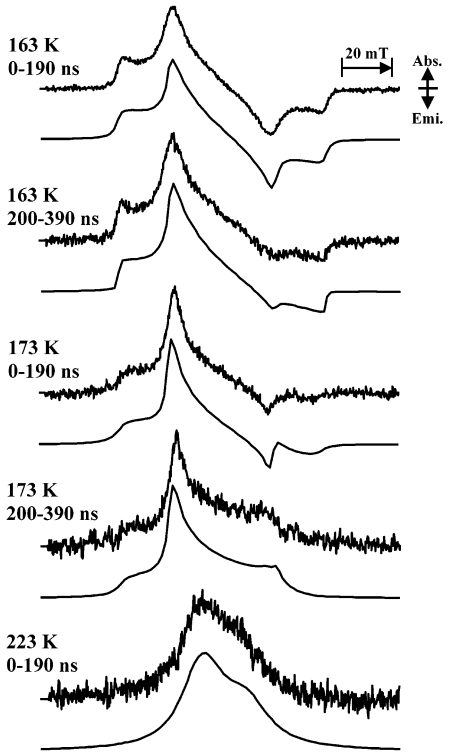

Figure 4. Experimentally obtained and simulated time-resolved EPR spectra of boronsubpthalocyanine boron chloride in the excited triplet state at 163−223 K in toluene.

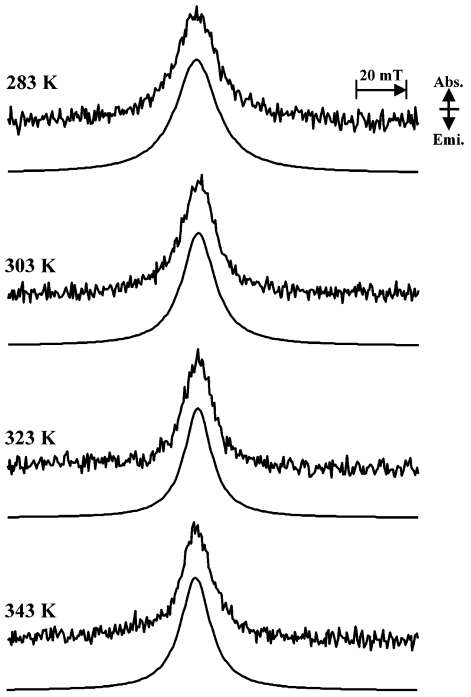

Figure 5. Experimentally obtained and simulated time-resolved EPR spectra of boronsubpthalocyanine boron chloride in the excited triplet state at 283−343 K in toluene.

The first method calculates the ZFS parameters by the half-point approximation[31] with the aid of the calculated geometry and electron distribution, as shown in Figures 1b and 2. Two transitions of 110−111 (E; **1**) and 110−112 (E; **2**) were assigned for two lower excited triplet states, ψ_{1T} and ψ_{2T}, with the calculated ZFS parameters $D_1 = D_2 = 25.9$, $E_1 = -E_2 = 5.0$ mT. The D value is the same for the two transitions and E has the same magnitude with different sign. These identical parameters reflect the high molecular symmetry of C_{3v}, which influences the electronic structures of the ^{1}T and ^{2}T states.

A different calculation of the ZFS parameters was carried out by the method of Higuchi[32] using the PPP LCAO MOs and approximate orthogonal AOs for planar SubPc^{2-}, where the B atom is removed from SubPc. In this calculation, we aimed at better fit of the obtained ZFS parameters and examining the effect of distortion due to the Jahn−Teller interaction. The procedure is the following: (1) The geometry is optimized by the use of B3LPY/6-31G* and then symmetrically adapted to the C_{3v} structure. (2) The PPP MO calculation, which includes several configuration interactions, gives rise to energies and electron distribution of the excited states in planar SubPc^{2-}. Under these assumptions, the values of D and E were calculated to be $D_1 = D_2 = 39.9$ and $E_1 = -E_2 = 6.3$ mT, for the ^{1}T and ^{2}T states, with $\theta = 120°$ ($\theta = < N_1BN_5$ in Figure 1a), where the C_{3v} symmetry is preserved. (3) To obtain the geometries of isosceles triangles with short (S) and long (L) bases, the molecular frame of C−N−C (A: 8−9−10, B: 12−2−2, C: 4−5−6 in Figure 1a) is changed from $\theta = 120$ to 117 (S) and 123° (L), respectively. In this case, the ZFS parameters were calculated to be $D_S = 38.8$, $E_S = 6.4$, $D_L = 38.7$, $E_L = 7.1$ mT for the two isosceles triangles. It is therefore found that D does not vary much (0.5%), whereas E varies more significantly (11%) with $\Delta\theta = \pm 3°$ because of the Jahn−Teller distortion.

c. TREPR Spectra and Their Simulation. TREPR spectra were measured and analyzed at 5−360 K in toluene. The obtained and simulated spectra are shown in Figures 3−5. Characteristic features in each temperature range are summarized below.

i. Solid Phase: 5−120 K.

Below 20 K, the observed spectra do not vary significantly and correspond to site I (Figure 3). The spectrum is simulated with the ZFS parameters $D = 35.8$ and $|E| = 8.4$ mT and an

TABLE 1: Static Parameters Obtained from Simulation of the Spectra at 20−120 K[a]

	species I, $D = 35.8$, $\|E\| = 8.4$ mT				species II, $D = 35.8$, $\|E\| = 11.9$ mT			
T/K	$\Delta\omega_x$[b]/mT	$\Delta\omega_y$[b]/mT	$\Delta\omega_z$[b]/mT	I/%	$\Delta\omega_x$[b]/mT	$\Delta\omega_y$[b]/mT	$\Delta\omega_z$[b]/mT	II/%
20	0.4	0.5	0.05	95	1.5	0.2	0.05	5
60	0.6	0.5	0.05	70	1.5	0.2	0.05	30
80	0.7	0.5	0.05	40	2.0	0.2	0.05	60
100	1	1	0.05	25	2.2	0.2	0.05	75
120	1.6	1	0.1	8	2.3	0.3	0.1	92

[a] With slow exchange rates; $k_{ex} = 1.7\ (60) - 3.3 \times 10^7\ s^{-1}$ (120 K). [b] Line width (eq 14).

TABLE 2: Dynamic Parameters Obtained from Simulation of the Spectra Observed at 0−190 ns after the Laser Pulse and 163−263 K[a]

T/K	$1/_{T2x}$[b]/mT	$1/_{T2y}$[b]/mT	$1/_{T2z}$[b]/mT	T_{1xy}/ns	T_{1z}/ns	T_{1d}[c]/ns	α/ degree	β/degree	γ/degree	$k_{ex}/10^8\ s^{-1}$
163	6	0.1	5.7	95	73	2100	90	3	3	3.3
173	8.3	0.1	23	59	45	950	90	6	2	12 (2.9)[d]
183	8.5	0.3	41	48	38	480	90	8	11	14 (5.6)
203	10	0.5	30	38	32	160	90	15	27	16 (17)
223	10	0.6	29	32	30	70	90	60	30	28 (39)
243	10	0.6	20	24	23	38	90	75	40	>28 (71)
263	10	5	20	<23	<23	24	90	85	75	>28

[a] Zero-field splitting parameters $D = 35.8$ and $|E| = 8.4$ mT. [b] $1/T_{2i} = 2\pi\Delta\omega_i$ ($i = x, y, z$; eq 14); $1/T_2$ of 10 mT corresponds to T_2 of 3.6 ns. [c] Calculated from eq 20 with $r = 4.5$ Å. [d] The values in parentheses are calculated from eq 16 and $k_{ex} = \tau_r^{-1}$ with $r = 4.5$ Å.

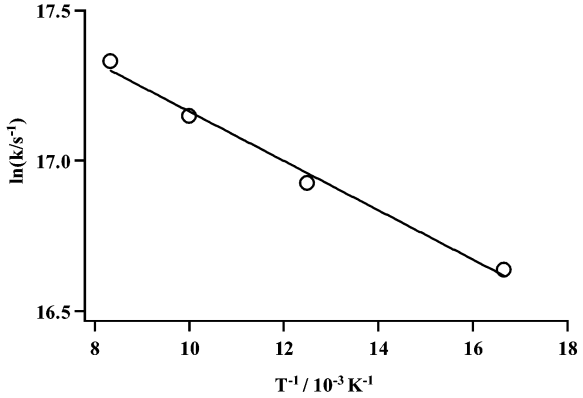

Figure 6. Arrhenius plots of k_{ex} obtained at 60−120 K.

intersystem crossing (ISC) ratio of $A_z - A_x$: $A_y - A_x = 1{:}0$. In view of similar porphyrins[33] and phthalocyanines[34] which exhibit $D > 0$, the T_z sublevel, which is selectively populated, is assumed to be the lowest energy level. In the temperature range of 40−120 K, the spectrum starts to change, loosing clear peaks in the canonical orientations $B//x$ and $B//y$, while the spectrum remains sharp at the *z* canonical orientation. The spectra were simulated by the two-site (I and II) model described in section 3. The parameters used in the simulation are $D_I = D_{II} = 35.8$ mT, $|E_I| = 8.4$, and $|E_{II}| = 11.9$ mT with slow exchange rates ($1.7 \times 10^7\ s^{-1}$ at 60 K and $3.3 \times 10^7\ s^{-1}$ at 120 K in Figure 6), where the species which corresponds to site II becomes more significant, as temperature rises (Table 1). All other simulated parameters are summarized in Table 1. The k_{ex} values are plotted in Figure 6 and analyzed by the equation:

$$k_{ex} = k_{ex}^{\ 0} \exp(-\Delta E/kT) \tag{11}$$

We obtained k_{ex}^0 and ΔE as $6.5 \times 10^7\ s^{-1}$ and 57 cm^{-1}, respectively. Thus, the two species are coexistent with a given ratio at each temperature.

ii. Liquid Phase: 130−260 K.

In the temperature range of 130−160 K, the spectra were not reproducible and were strongly dependent upon the cooling rate, cooling direction, and sample orientation. This is a rather typical phenomenon in the soft glass region of toluene,[5,9] which prevented us from simulating the spectra at this temperature range. At around 163 K, the spectrum shows a typical pattern of $E = 0$ and continues to vary remarkably for temperature above 170 K, still exhibiting some structure up to 243 K (Figure 4). The spectral simulation in this temperature range was examined with the two-site discrete jump model described in section 3, and one site is sufficient for obtaining the simulation results, as shown in Figure 4. The spin−lattice relaxation time (T_{1i}; $i = x, y, z$) was obtained from the decay curve of the signal at each stationary field ($B// x, y, z$) under a condition that the spin relaxations are fast enough as compared with the strength (B_1) of microwave ($\gamma B_1 T_1 T_2 \ll 1$).[35] Alternatively, T_1 can be obtained directly from the simulation of the spectra, as one of the fitting parameters (see above). The best-fit parameters obtained from the decay curve (which are similar to the ones obtained from the simulation of the spectra) are summarized in Table 2. The same values of *D*, $|E|$, and A_i ($i = x, y, z$) were used at all temperatures. Under these conditions, the spectrum is highly sensitive to *D* and A_i but less sensitive to $|E|$. On the basis of our spectral simulation, we concluded that *D* and A_i do not depend on temperature. Although the results are reported for a single $|E|$ value, we do believe that the two molecular sites having different *E*, observed at lower temperatures, are involved in the spectra. Despite the possible existence of two sites, the fast rotation about the molecular *z*-axis makes the spectra less sensitive to changes in $|E|$, and, as mentioned above, can be simulated with a single $|E|$ value. The parameters k_{ex}, α, β, and γ, which are also sensitive parameters, enable us to estimate the exchange and rotational rates $k_{||}$ and $k_\perp$ for the in-plane and out-of-plane motions, respectively, which reflect the intramolecular dynamics. The values were calculated by eqs 12 and 13 and are summarized in Table 3.

$$k_{||} = k_{ex}\,(\alpha/57°) \tag{12}$$

$$k_\perp = k_{ex}\,(\beta/57°) \tag{13}$$

From Table 3, it is found that the intramolecular motion is highly anisotropic at lower temperatures, for example, $k_{||}/k_\perp = 30$ at 163 K, and becomes nearly isotropic at higher temperatures, $k_{||}/k_\perp = 1.2$ at 243 K. From the Arrhenius plots, the activation energies were obtained for the two processes, that

TABLE 3: Anisotropic Exchange Rate Constants

T/K	$k_{\parallel}/10^8 s^{-1}$	$k_{\perp}/10^8 s^{-1}$	$k_{\parallel}/k_{\perp}$
163	5.2	0.17	30
173	19	1.3	15
183	22	2.0	11
203	24	4.1	5.9
223	44	29	1.5
243			1.2[a]

[a] Obtained from α/β in Table 2.

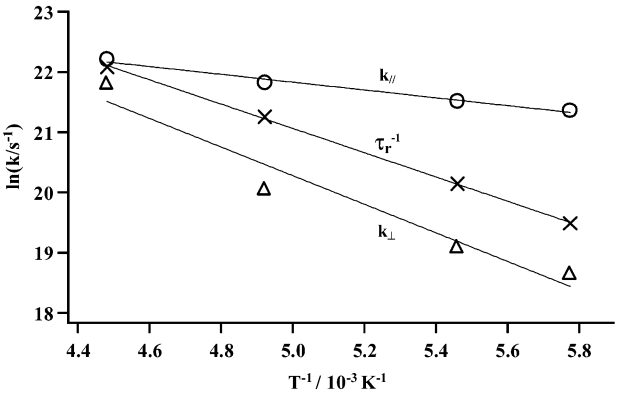

Figure 7. Arrhenius plots of $k_{\parallel}$ (in-plane), $k_{\perp}$ (out-of-plane motions), and τ_r^{-1}.

TABLE 4: Experimentally Obtained (T_2) and Calculated (T_{2d}) Spin−Spin Relaxation Times

T/K	$\Delta\omega$[a]/mT	T_2[b]/ns	T_{2d}[c]/ns
283	3.6	1.6	1.6
303	2.9	2.0	1.9
323	2.5	2.3	2.2
343	2.4	2.4	2.5

[a] Half-width at the half-maximum. [b] Calculated from eq 14. [c] Calculated from eq 15 with $r = 4.5$ Å.

is, the in-plane ($k_{\parallel}$) and out-of-plane ($k_{\perp}$) rotations (Figure 7). These values were calculated to be ca. 420 and 1620 cm^{-1} for the in-plane and out-of-plane rotations, respectively.

iii. Liquid Phase: 270−370 K.

In this temperature range, the spectrum has lost all its structure and is characterized by a single peak, as shown in Figure 5. These spectra were analyzed with a simple Lorentzian line shape simulation. From the half width at half-maximum ($\Delta\omega$/mT) of the simulated spectrum, the spin−spin relaxation time, T_2, is obtained by eq 14 and summarized in Table 4.

$$T_2 = 1/2\pi\Delta\omega \qquad (14)$$

T_1 is not obtained in this temperature range because time resolution of our system (ca. 80 ns) cannot trace the fast T_1 process (<20 ns in Table 2).

5. Discussion

a. Simulation Procedure. The triplet line shape simulation for the low-temperature spectra requires eight independent parameters (six T_2 values for the two species, fraction of each species, and the exchange rate). The simulation ignores the effects of *g* and hyperfine coupling (hfc) anisotropy. Inclusion of these parameters would add at least six additional independent parameters depending on the exact model. It is obvious that additional parameters would make the simulation process impossible (computationally) and meaningless (physically) because various combinations of parameters would provide very similar and undistinguishable results. Therefore, we consider the T_2 values given for the spectra at low temperature as an "effective T_2", which includes all the additional Hamiltonian terms that we have ignored. The effective T_2 is close to the real T_2 of the species, only in the case where *g*, hfc, and other second-order terms in the Hamiltonian are relatively small. Nevertheless, one property that this effective T_2 does not account for is the exchange rate between the sites. The spectra could have been simulated using Gaussian lines with effective line widths that account for all second-order terms in the Hamiltonian including the exchange. In such a fitting process, one cannot obtain the exchange rate from the simulation, as it is hidden within the effective line width of the Gaussian line shape. In the present simulation scheme, the exchange is treated separately from T_2, thus enabling to obtain good estimate of the exchange rate between the two sites at various temperatures. For the temperature range $T > 160$ K, the values of $1/T_2$, at various canonical orientations, are usually large enough to account for the observed line width. Thus, in fluid solution, the effective T_2 can be considered in most cases as the real T_2 of the species.

b. Electronic Structures at Lower Temperature. Two kinds of triplet species were observed at 40−120 K, having nearly the same *D* but different |*E*| values ($D_I = D_{II} = 35.8$ mT, $|E_I| = 8.4$, and $|E_{II}| = 11.9$ mT). The observed none-zero *E* value indicates that the ^{1}T structures are distorted from the C_{3v} symmetry, as expected from the Jahn−Teller splitting. Here, we compare the observed values described above with the calculated ones in section 4a ($D_S = 38.8$, $E_S = 6.4$, $D_L = 38.7$, $E_L = -7.1$ mT); the value of *D* remains the same and *E* varies with the Jahn−Teller distortion. Therefore, we can conclude that the two observed sites at 40−120 K correspond to those of the Jahn−Teller states.

Jahn−Teller splitting for the EPR spectra at low temperatures has been reported in several systems of the ^{1}T state such as benzene,[36] metalloporphyrins,[37] and fullerene.[38] For the fullerene triplet, Bennati et al. analyzed the temperature dependence of the EPR spectra with the exchange rate of $(2.5-7) \times 10^7$ s^{-1} at 20−80 K and interpreted in terms of the tunneling process between the Jahn−Teller split states.[38] The rates they obtained are close to ours ($1.7-3.3 \times 10^7$ s^{-1} at 40−120 K) and a similar process must occur for C_{60} and SubPc in the ^{1}T state. In metalloporphyrins, a similar activation energy (30−70 cm^{-1}) was also obtained for the Jahn−Teller states.[39] These facts confirm our assignment that the Jahn−Teller states are involved in this temperature range.

The *D* value we have found is larger than those of porphyrins (32−34 mT)[39] and phthalocyanines (25−28 mT),[34] reflecting the relative small size of this molecule. The fact that *D* is independent of temperature is consistent with the calculation (section 4a) that the other excited states are located far above the lowest ^{1}T state. If the nearby ^{2}T states or other conformers were located close to the ^{1}T state, a temperature dependence of *D* should have been observed as reported in the literature.[4,8,9]

The triplet spectrum of subphthalocyanine bromide, in frozen solution, was reported earlier,[19] with ZFS parameters a little different ($D = 31.0$ and $|E| = 4.3$ mT) from ours. The population from the lowest excited singlet (^{1}S) state was selective and dominant to the lowest T_z sublevel. These two facts could be interpreted in terms of a heavy atom effect, namely, a spin−orbit coupling on the axially ligated halogen atom. This resembles the case of the external heavy atom effect of the halogen atom on the $\pi\pi^*$ triplet molecules. Here, the halogen atom is located just above the aromatic plane and a spin−orbit coupling of the *z* component increases, inducing T_z preference and a decrease in *D*.[40] The spin−orbit coupling on

the C*l* atom ($\varsigma = 586$ cm^{-1}) prevails over that of the boron atom (11 cm^{-1}).

c. Dynamic Properties at Elevated Temperatures. At temperatures above 273 K, the spectra exhibit a homogeneous line shape, from which the isotropic spin−spin relaxation time, T_2, can be extracted (Table 4).[41] For a rotating triplet molecule in solution, T_{2d} can be calculated on the basis of the spin dipolar interaction model using the equations[42]

$$T_{2d}^{-1} = 1/15 \cdot D^{*2}\tau_r [3 + 5/(1 + \nu^2\tau_r^2) + 2/(1 + 4\nu^2\tau_r^2)] \quad (15)$$

$$\tau_r = (4/3)\pi\eta r^3/kT \quad (16)$$

where D^* [$= (D^2 + 3E^2)^{1/2}$] and τ_r denote the effective ZFS parameter and the rotational correlation time,[43] respectively, η is the viscosity, r is the hydrodynamic radius of the molecule, ν is the microwave frequency, and k is the Boltzmann constant. The best-fit T_{2d} values were obtained using $r = 4.5$ Å (Table 4). The coincidence between the observed and calculated values is satisfactory, and the value of 4.5 Å is fairly reasonable[11] as seen in Figure 1a. Another transverse mechanism, via spin−rotation interactions, can also be considered by using the equations[44]

$$T_{2r} = T_{1r} = 9\tau_r/(\Delta g_{||}^2 + \Delta g_{\perp}^2) \quad (17)$$

$$\Delta g_{||} = g_{||} - g_e \quad (18)$$

$$\Delta g_{\perp} = g_{\perp} - g_e \quad (19)$$

where g_e is the free-electron g value (2.0023). Inserting $\Delta g_{||} = \Delta g_{\perp} = 0.003$ (which is the largest possible value[45]) and $r = 4.5$ Å, we obtain $T_{2r} = 15\ \mu$s, which is much longer than T_{2d} (Table 4), thus implying that this mechanism is negligible in our case. We can conclude that at temperature above 280 K, the SubPc behaves as a spherical molecule and the line shape is governed through the spin dipolar interaction in the triplet state.

The spin−lattice relaxation time, T_{1d}, due to the spin dipolar interactions, is calculated by[40]

$$T_{1d}^{-1} = 2/15 \cdot D^{*2}\tau_r [1/(1 + \nu^2\tau_r^2) + 4/(1 + 4\nu^2\tau_r^2)] \quad (20)$$

The values of T_{1d} were calculated using $r = 4.5$ Å and are summarized in Table 2. Notice that the T_1 values from the simulation are much smaller (<1/10) than those for temperatures lower than 183 K. We attribute this discrepancy to the anisotropic (in-plane) rotations or pseudorotations that cause much faster motion than that calculated for a spherical molecule. To test the effect of molecular rotations on the spectral changes, let us compare the obtained anisotropic exchange rate constants $k_{||}$ and $k_{\perp}$ (Table 3) with the isotropic rotational correlation rate τ_r^{-1}. The values of τ_r^{-1} were calculated for different temperatures using eq 16 with $r = 4.5$ Å and are summarized in Table 2 and plotted in Figure 7. Inspection of Figure 7 reveals that τ_r^{-1} and $k_{\perp}$ exhibit similar activation energy. This implies that the out-of-plane rotations are real rotations and not pseudorotations.[46] For the in-plane exchange, two possibilities are considered, that is, the in-plane rotation and the Jahn−Teller averaging. The activation energies (E_a) for anisotropic rotation in solid neat benzene[47] were 286 and 1120 cm^{-1}. These results are similar to the values 420 and 1620 cm^{-1}, obtained in our study. On the other hand, the anisotropy of $k_{||}/k_{\perp}$ is larger (>10 at T < 183 K) than that (<3) found in benzene (2.3 at $T \sim 280$ K).[46] Such a small anisotropy could also be calculated from the molecular shape,[48] where $r_l/r_s \sim 2.1$ (Figure 1b, where l and s denote the long and short axis, respectively). Therefore, the fast in-plane exchange at <200 K (Table 3) does not originate from the in-plane rotation but from the Jahn−Teller averaging, that is, pseudorotations. Above 200 K, the observed small anisotropy of $k_{||}/k_{\perp} \sim 1.5$ could be explained by the real rotation of SubPc.

The relaxation times we obtained for SubPc can be compared to those of triplet fullerene. In $^3C_{60}$*, T_1 and T_2 were interpreted through the temperature dependence of the spin dipolar process (eqs 15 and 20) at 170−220 K but not at higher temperatures. In our case, however, the spin dipolar process explains well the relaxation times obtained at high temperatures (Tables 2 and 4), and the exchange between Jahn−Teller states was the dominant process at low temperatures.[14] The apparent discrepancies may be interpreted through the very high pseudorotation rate of $^3C_{60}$*, which results in a small effective D^* (2.2 mT [5,13]) at high temperature, as compared with $D^* \sim 40$ mT for triplet SubPc.

6. Conclusion

TREPR spectra of photoexcited triplet SubPc was measured over a wide temperature range of 5−360 K. The spectra were analyzed both in the solid and fluid phases of toluene, in terms of a static and dynamic Jahn−Teller interaction combined with anisotropic molecular rotations. We have shown that the EPR spectra can be used to obtain the energy difference and the exchange rate between two sites even in the fluid phase. Moreover, from the spectra simulated we could extract the exchange or dynamic rotational rates as well as the various magnetic parameters of this interesting molecule.

Acknowledgment. This work is supported by a Grant-in-Aid for Scientific Research No. 10044057 and 12440157 from the Ministry of Education, Science, Sports, and Culture, Japan. This work was partially supported by the Israel Ministry of Science, through the "Eshkol Foundation Stipends" (A. B.), by a US−Israel BSF grant 1999-041, and by an Israeli Ministry of Science grant No. 1485-2-00. The Farkas Research Center is supported by the Bundesministerium für die Forschung und Technologie and the Minerva Gesellschaft für Forchung GmbH, FRG. S.Y. and A.T. thank Dr. Junichi Fujisawa at Riken for his support at an earlier stage of the experiment.

References and Notes

(1) Hirota, N.; Yamauchi, S. In *Dynamic Spin Chemistry*; Kuchitsu, K., Ed.; Kodansha: Tokyo, 1998; p 187−248.
(2) Rassat, A.; Marx, L *Angew. Chem., Int. Ed.* **2000**, *39*, 4494.
(3) Thomson, C *J. Chem. Phys*. **1964**, *41*, 1.
(4) Ong, J-L.; Sloop, J.; Lin, T-S. *J. Phys. Chem.* **1992**, *96*, 4762.
(5) Levanon, H.; Meiklyar, V.; Michaeli, A.; Michaeli, S.; Regev, A. *J. Phys. Chem*. **1992**, *96*, 6128. Regev, A.; Gamliel, D.; Meiklyar, V.; Michaeli, S.; Levanon, H. *J. Phys. Chem.* **1993**, *97*, 3671.
(6) Kim, S. S.; Tsay, F-D.; Gupta, A. *J. Phys. Chem*. **1987**, *91*, 4851.
(7) Sieckmann, I.; Brettel, K.; Bock, C.; van der Est, A.; Stehlik, D. *Biochemistry* **1993**, *32*, 4842.
(8) Kamei, T.; Terazima, M.; Yamauchi, S.; Hirota, N. *J. Phys. Chem.* **1994**, *98*, 7963.
(9) Kay, C. W. M.; Elger, G.: Moebius, K. *Phys. Chem. Chem. Phys.* **1999**, *1*, 3999.
(10) Closs, G. L.; Gautam, P.; Zhang, D.; Krusic, P. J.; Hill, S. A.; Wasserman, E. *J. Phys. Chem.* **1992**, *96*, 5228. Terazima, N.; Hirota, H.; Shimohara, Y.; Saito, Y. *Chem. Phys. Lett.* **1992**, *195* 333; Zhang, D; Norris, J. R.; Krusic, P. J.; Wasserman, E.; Chen, C.-C.; Lieber, C. M. *J. Phys. Chem*. **1993**, *97*, 5886.
(11) McLauchlan, K. A.; Shkrob, L. A.; Yeung, M. T. *Chem. Phys. Lett.* **1994**, *217*, 157.
(12) Fujisawa, J.; Ishii, K.; Ohba, Y.; Iwaizumi, M.; Yamauchi, S. *J. Phys. Chem.* **1995**, *99*, 17084. Fujisawa, J. I.; Ohba, Y.; Yamauchi, S. *J.*

Phys. Chem. **1997**, *101*, 434. Fujisawa, J.; Ohba, Y.; Yamauchi, S. *J. Phys. Chem. A* **1997**, *119*, 8736.
(13) Saiful, I. S. M.; Fujisawa, J.; Kobayashi, N.; Ohba, Y.; Yamauchi, S. *Bull. Chem. Soc. Jpn.* **1999**, *72*, 661.
(14) Steren, C. A.; van Willigen, H.; Dinse, K.-P. *J. Phys. Chem.* **1994**, *98*, 7464.
(15) Gonen, O.; Levanon, H. *J. Chem. Phys.* **1986**, *84*, 4132. Levanon, H. *Rev. Chem. Intermed.* **1987**, *8*, 287.
(16) Schneider, D. J.; Freed, J. H. *Adv. Chem. Phys.* **1989**, *73*, 387. Gamliel, D.; Levanon, H. *J. Chem. Phys.* **1992**, *97*, 7140.
(17) Regev, A.; Gamliel, D.; Meiklyar, V.; Michaeli, S.; Levanon, H. *J. Phys. Chem.* **1993**, *97*, 3671.
(18) Kudrevich, S. V.; Gilbert, S.; van Lier, E. *J. Org. Chem.* **1996**, *61*, 5706.
(19) Kobayashi, N.; Ishizaki, T.; Ishii, K.; Konami, H. *J. Am. Chem. Soc.* **1999**, *121*, 9096.
(20) Diaz-Garcia, M. A.; Agullo-Lopez, F.; Sastre, A.; Torres, T.; Torruellas, W. E.; Stegeman, G. I. *J. Phys. Chem.* **1995**, *99*, 14988.
(21) Hunt, H. Brit. U.K. Pat. Appl. GB 2290489 A1 3 Jan **1995**, 22.
(22) Frisch, M. J.; Trucks, G. W.; Schlegel, H. B.; Scuseria, G. E.; Robb, M. A.; Cheeseman, J. R.; Zakrzewski, V. G.; Montgomery, J. A., Jr.; Stratmann, R. E.; Burant, J. C.; Dapprich, S.; Millam, J. M.; Daniels, A. D.; Kudin, K. N.; Strain, M. C.; Farkas, O.; Tomasi, J.; Barone, V.; Cossi, M.; Cammi, R.; Mennucci, B.; Pomelli, C.; Adamo, C.; Clifford, S.; Ochterski, J.; Petersson, G. A.; Ayala, P. Y.; Cui, Q.; Morokuma, K.; Malick, D. K.; Rabuck, A. D.; Raghavachari, K.; Foresman, J. B.; Cioslowski, J.; Ortiz, J. V.; Baboul, A. G.; Stefanov, B. B.; Liu, G.; Liashenko, A.; Piskorz, P.; Komaromi, I.; Gomperts, R.; Martin, R. L.; Fox, D. J.; Keith, T.; Al-Laham, M. A.; Peng, C. Y.; Nanayakkara, A.; Gonzalez, C.; Challacombe, M.; Gill, P. M. W.; Johnson, B.; Chen, W.; Wong, M. W.; Andres, J. L.; Gonzalez, C.; Head-Gordon, M.; Replogle, E. S.; Pople, J. A. Gaussian 98; Gaussian, Inc.: Pittsburgh, PA.
(23) Kietaibl, H. *Monatsh. Chem.* **1974**, *105*, 405.
(24) Hudson, A.; McLachlan, A. D. *J. Chem. Phys.* **1965**, *43*, 1518.
(25) Levanon, H.; Vega, S. *J. Chem. Phys.* **1974**, *61*, 2265.
(26) Shain, A. L. Ph.D. Dissertation, Washington University, 1968. Shain, A. L. *J. Chem. Phys.* **1972**, *56*, 6201. Wasserman, E.; Snyder, L. C.; Yager, W. A. *J. Chem. Phys.* **1964**, *41*, 1763.
(27) Regev, A.; Galili, T.; Levanon, H.; Harriman, A. *Chem. Phys. Lett.* **1986**, *131*, 140.
(28) Kubo, R.; Tomita, J. *J. Phys. Soc. Jpn.* **1954**, *9*, 888.
(29) Hiromitsu, I.; Kevan, L. *J. Chem. Phys.* **1988**, *88*, 691.
(30) Gonen, O.; Levanon, H. *J. Phys. Chem.* **1984**, *88*, 4223.
(31) Higuchi, J. *J. Chem. Phys.* **1963**, *38*, 1237; **1963**, *39*, 1339; **1963**, *39*, 1847.
(32) Higuchi, J. *Bull. Chem. Soc. Jpn.* **1981**, *54*, 2864; **1982**, *55*, 1961.
(33) Langoff, S. R.; Davidson, E. R.; Gouterman, M.; Leenstra, W. R.; Kwiram, A. L. *J. Chem. Phys.* **1975**, *62*, 169.
(34) Miyamoto, R.; Yamauchi, S.; Kobayashi, N.; Osa, T.; Ohba, Y.; Iwaizumi, M. *Coord. Chem. Rev.* **1994**, *132*, 57.
(35) Furrer, R; Fujara, F.; Lange, C.; Stehlik, D.; Vieth, H. M.; Vollmann, W. *Chem. Phys. Lett.* **1980**, *75*, 332.
(36) de Groot, D. M.; Hesselmann, I. A. M.; van der Waals, J. H. *Mol. Phys.* **1969**, *16*, 45.
(37) Canters, G. W.; Jansen, G.; Noort, M.; van der Waals, J. H. *J. Phys. Chem.* **1976**, *80*, 2253. Scherz, A.; Levanon, H. *J. Phys. Chem.* **1980**, *84*, 324.
(38) Bennati, M.; Grupp, A.; Mehring, M. *J. Chem. Phys.* **1995**, *102*, 9457.
(39) Yamauchi, S.; Matsukawa, Y.; Ohba, Y.; Iwaizumi, M. *Inorg. Chem.* **1996**, *35*, 2910.
(40) Komada, Y.; Yamauchi, S.; Hirota, N. *J. Chem. Phys.* **1985**, *82*, 1651.
(41) For different relaxation mechanisms, which operate simultaneously, the relaxation rates obey $1/T_2 = \Sigma_i 1/T_{2i}$ and $1/T_1 = \Sigma_i 1/T_{1i}$.
(42) Carrington, A.; McLauchlan, A. D. *Introduction to Magnetic Resonance*; Harper & Row: New York, 1967; p 201.
(43) Debye, P. *Polar Molecule*; Dover Publications: New York, 1929.
(44) Atkins, P. W.; Kivelson, D. *J. Phys. Chem.* **1966**, *44*, 169.
(45) Ishii, K.; Ohba, Y.; Iwaizumi, M.; Yamauchi, S. *J. Phys. Chem.* **1996**, *100*, 3839.
(46) Meakins, R. J. *Trans. Faraday Soc.* **1958**, *54*, 1160.
(47) Witt, R.; Sturz, L.; Dolle, A.; Muller-Plathe, F. *J. Phys. Chem. A* **2000**, *104*, 5716.
(48) Böttcher, C. J. F.; Bordwijk, P. In *Theory of Electric Polarization Vol. 2*; Elsevier: Amsterdam, 1978; p 202.